Catching the Role of Anisotropic Electronic Distribution and Charge Transfer in Halogen Bonded Complexes of Noble Gases

Alessio Bartocci,[1] Leonardo Belpassi,[2] David Cappelletti,[1] Stefano Falcinelli,[3] Felice Grandinetti,[4] Francesco Tarantelli,[1] and Fernando Pirani[1]

[1)] *Dipartimento di Chimica, Biologia e Biotecnologie, Università di Perugia, 06123, Italy*

[2)] *Istituto di Scienze e Tecnologie Molecolari del CNR, Perugia, 06123, Italy*

[3)] *Dipartimento di Ingegneria Civile ed Ambientale, Università degli Studi di Perugia, 06125 Perugia, Italy*

[4)] *Dipartimento per la Innovazione nei sistemi Biologici, Agroalimentari e Forestali (DIBAF), Università della Tuscia,01100 Viterbo, Italy*

The systems studied in this work are gas-phase weakly-bound adducts of the noble-gas atoms with CCl_4 and CF_4. Their investigation was motivated by the widespread current interest for the intermolecular halogen bond (XB), a structural motif recognized to play a role in fields ranging from elementary processes to biochemistry. The simulation of the static and dynamic behavior of complex systems featuring XB requires the formulation of reliable and accurate model potentials, whose development relies on the detailed characterization of strength and nature of the interactions occurring in simple exemplary halogenated systems. We thus selected the prototypical Ng-CCl_4 and Ng-CF_4, and performed high-resolution molecular-beam scattering experiments to measure, the absolute scale of their intermolecular potentials, with high sensitivity. In general, we expected to probe typical van der Waals (vdW) interactions, consisting of a combination of size (exchange) repulsion with dispersion/induction attraction. For the He/Ne-CF_4, the analysis of the glory quantum interference pattern, observable in the velocity dependence of the integral cross section, confirmed indeed this expectation. On the other hand, for the He/Ne/Ar-CCl_4, the scattering data unravelled much deeper potential wells, particularly for certain configurations of the interacting partners. The experimental data can be properly reproduced only including a shifting of the repulsive wall at shorter distances, accompanied by an increased role of the dispersion attraction, and an additional short-range stabilization component. To put these findings on a firmer ground, we performed, for selected geometries of the interacting complexes, accurate theoretical calculations aimed to evaluate the intermolecular interaction and the effects of the complex formation on the electron charge density of the constituting moieties. It was thus ascertained that the adjustments of the potential suggested by the analysis of the experiments actually reflect two chemically-meaningful contributions, namely a stabilizing interaction arising from the anisotropy of the charge distribution around the Cl atom in CCl_4, and a stereospecific electron transfer that occurs at the intermolecular distances mainly probed by the experiments. Our model calculations suggest that the largest effect is for the vertex geometry of CCl_4 while other geometries appears to play a minor to negligible role.

I. INTRODUCTION

Intermolecular and/or intramolecular halogen bonding (XB) formation has a long history, dating back more than one century ago[1–3]. In general, this structural motif relies on the favorable interaction between an "electrophilic halogen atom and a nucleophilic region in another, or in the same molecular entity"[4]. It was, however, only in the last two decades[5] that the directionality and strength of the XB (which typically ranges between 5 and 180 kJ/mol) were recognized as key factors in molecular recognition and crystal packing[6,7], playing a crucial role, for example, in crystal engineering, superconductors, liquid crystals, nanoparticles, and drug design.

XB has many analogies with hydrogen bond (HB)[8–17]. For example the stenght of both HB and XB, at intermediate and large intermolecular distances, is determined by a delicate balance of interaction components such as size repulsion, dispersion and induction attraction, charge transfer (CT), and electrostatic [18]. However, XB has the peculiar contribution of the so-called "σ hole"[8,16,17,19–22] and "polar flattening" (PF)[8,23–28]. Specifically, σ-hole is a localized region showing a net positive electrostatic potential, which drives the approach of an XB donor to an electron-rich acceptor. The magnitude of the σ-hole is strictly related to the strength of the electrostatic interaction energy, even if this component alone is not able to explain all the characteristics of XBs.[29–33] Therefore, the proper understanding and description of σ-hole is of primary importance to model XB. The polar flattening is related to the "effective" shape of the halogen atom in the molecular entity and its contribution is expected to affect mainly the anisotropy of size repulsion term of the interaction.[26–28] The proper modelling of PF appears crucial to describe position and strength of the repulsive wall in X-bonds and then the structures in biomolecular systems.[26,28] We mention that the σ hole and PF have a common origin, i.e. the electronic charge distribution that, in covalently bounded systems containing heavier halogen atoms, presents a significant distorsion (flattening) especially in the outer part of halogen in the direction of an approaching electron donor.

XB was already investigated by various theoretical methods (see refs.[8–17,27,29–33] and references therein), but the experimental evidence is still limited. The available results come mostly from studies in solution[34–37] and analysis of crystallographic structural data[38–40], as well as from gas-phase experiments performed by microwave-rotational spectroscopy[1,41].

Scattering data are available only for few systems[42], and measurements of the absolute scale of the interactions are still lacking.

CCl_4 and CF_4 are prototypical apolar halogenated molecules usually assumed to be hydrophobic [43–45]. Due to the high symmetry (Td), the terms contributing to intermolecular bonds[46,47] involving CCl_4 and CF_4 are, in general, relatively few, and, in particular, the complexes with the noble-gas atoms (Ng) feature the absence of electrostatic effects, arising from the interaction between permanent charges and/or permanent dipole and quadrupole, and an expected minor role of induction. Therefore, the Ng-CX_4 (X = Cl, F) interaction, up to date unexplored, is expected to be representative of the anisotropic character of the ubiquitous van der Waals (vdW) component (defined here for convenience as size repulsion plus dispersion attraction) in halogenated molecular systems. It is also of interest to assay the conceivable role of CT as a stabilizing contribution in the perturbative limit[48]. Overall, the Ng-CCl_4 and Ng-CF_4 appear as simple model systems suitable to mimic the intermolecular interactions occurring in halogenated molecules of higher complexity. In the present study, we discuss molecular beam (MB) scattering experiments aimed to measure the total (elastic plus inelastic) integral cross section $Q(v)$ as a function of the MB velocity v for some Ng-CCl_4 and Ng-CF_4 systems. The use of high velocity and high angular resolution allowed to resolve the oscillatory "glory" pattern, an important quantum interference structure observable in the velocity dependence of the integral cross section. The glory interference depends on phase shifts associated with partial waves of intermediate orbital angular momentum ℓ values. From a semiclassical point of view they correspond to trajectories at intermediate impact parameters b and at nearly zero deflection angle, for which attraction and repulsion balance their opposite effects, interfering with trajectories at impact parameters so large that the effect of the potential is negligible. The high resolution measurements of the glory pattern represent a relevant experimental tool since it strictly depends on the features of the interaction in the potential well, in particular on the well depth and on its location[49].

The obtained data furnished information on the absolute scale of the total intermolecular potential, and on its radial and angular dependencies (i.e. on the potential energy surface "PES"). In addition, working in an internally consistent way, it was possible to unravel intriguing differences between the Ng-CCl_4 and Ng-CF_4. Like previous studies from our laboratory[50–55], the MB experiments were corroborated by ab-initio calculations, performed to characterize the most relevant minima in the PESs, and to evaluate their electron density,

particularly in the comparison with that of the constituting moieties. This joint experimental and theoretical approach was recently employed to assay the effect of CT in the formation of weak HB[50,55]. Interestingly, in the present study, we found, in particular, that all the Ng-CCl_4 feature indeed an appreciable CT, including the complex with the most inert and, in principle, less nucleophilic helium. A preliminary analysis of lighter noble gas atoms scattering data have been anticipated in a recent paper.[56]

The paper is organized as follows. Section II summarizes the experimental methodologies, and reports the measured cross sections. Section III describes the formulation of the PES, and the analysis of the experimental data, which are discussed in Section IV based also on the theoretical calculations. The conclusions are summarized in Section V.

II. EXPERIMENTAL METHODS AND RESULTS

The employed MB apparatus was extensively described previously[57], and a sketch including key features relevant for the present investigation is given in Figure S1 of the Supplementary Material[58]. Briefly, the instrument operates under high angular and velocity resolution conditions[57], and allows to measure the integral cross section Q as a function of the selected MB velocity v. The fundamental quantity at each selected nominal velocity v is the MB attenuation I/I_0, I and I_0 being, respectively, the MB intensity detected in the presence and in the absence of the target in the scattering chamber. I/I_0 is related to the integral cross section $Q(v)$ through the Lambert-Beer law

$$Q(v) = -\frac{1}{NL} \log \frac{I}{I_0} \ , \tag{1}$$

where N is the target gas density and L the path length of the scattering region[57], both calibrated as discussed previously in References[59–61].

The $Q(v)$ values of NG-CF_4 and NG-CCl_4 (NG=He,Ne and Ar), plotted as a function of the selected MB velocity v, are reported in Figures 1 and 2. In Figure 2 the cross sections are plotted as $Q(v)v^{\frac{2}{5}}$ to emphasize the well resolved oscillatory patterns due to the "glory" quantum interference. In the case of the $ArCCl_4$ system the quantum interferences appear to be strongly quenched due to the significant role of interaction anisotropy, as suggested by the scattering calculations, discussed below. The data obtained for the various systems, are, in general, quite different both in the absolute scale and in the glory interference,

suggesting the occurrence of pronounced differences in the intermolecular interactions both at the long range, and at around the potential well[62,63]. During the analysis, the center-of-mass cross sections were calculated within the semiclassical JWKB method[64] from the assumed intermolecular interaction V (see next section), and eventually convoluted in the laboratory frame (see[58]) to directly compare them with the measured $Q(v)$.

III. REPRESENTATION OF THE PES AND DATA ANALYSIS

It was demonstrated previously[50,54,55] that the scattering of fast-rotating and randomly-oriented light molecules by atomic targets is mostly elastic, and driven by an effective potential that exhibits, at intermediate and large intermolecular distances, only a radial dependence. Therefore, such molecules essentially behave as pseudo-atoms (defined as single interaction centers) in the formed weakly-bound "floppy" systems, and their measured cross sections are properly analyzed under this assumption. The intermolecular potential V of heavy and large polyatomic molecules is, instead, only poorly described by a single interaction center located on the center-of-mass (CM). In particular, for the presently-investigated Ng-CCl_4 and Ng-CF_4, we assumed several interaction centers, one located on the Ng atom and the other on the molecular frame. The interaction is thus determined by an atom-effective molecular-size repulsion[65,66], strongly dependent on the molecular orientation, and by a global attraction arising from the combination of atom-bond contributions[66,67]. Such a formulation indirectly accounts for the electronic charge distribution of the molecular frame, and, therefore, furnishes a realistic description of the potential energy anisotropy. In particular, the partition of the molecular polarizability in bond tensor components allows a realistic picture of both the repulsion and the attraction of the ubiquitous van der Waals (V_{vdW}) interaction, as well as the inclusion of three body and other non-additive effects[67]. The performance of this formulation was already extensively tested by comparison with ab-initio calculations (see e.g. refs.[51,68–71]).

The interaction centers of the Ng-CCl_4 and Ng-CF_4 were located, in particular, on the Ng atom and on the C-Cl and C-F bonds, and V_{vdW} was formulated as a sum of four atom-bond interaction terms, each one being expressed by an Improved Lennard Jones (ILJ) function (details are given in Refs.[63,67] and references therein). The latter depends on r, the distance of the atom from the interaction center on each bond, and on α, the angle between the vector

r and the axis of the bond. The ILJ function is largely employed to probe the dynamics of atomic and molecular clusters (neutral and ionic) (see e.g. refs.[70,72–74]), and further details on its formulation are given in[58]. The interaction centers on the C-F and C-Cl bonds were located in proximity of the halogen atom, at about 60% and 80%, respectively, of the bond length. Such positions were estimated from the weighted average of the atomic polarizability contributions from the C atom (0.44 Å^3 for each bond)[75] and Cl (2.18 Å^3)[76] to the average C-Cl bond polarizability (2.62 Å^3), while for C-F the value, it has been exploited the F atom polarizability (0.56 Å^3)[75] in addition to that of C.

TABLE I. Zero order and adjusted (final) values of potential parameters (ε in meV and r_m in Å) for the He, Ne-CF and He, Ne, Ar-CCl atom-bond pairs. Maximum estimated uncertainty is 6% for ε, 2% for r_m and 10-15% for A.

Atom-bond pair		zero order				final				
		$r_{m\parallel}$	$\varepsilon_\parallel$	$r_{m\perp}$	$\varepsilon_\perp$	$r_{m\parallel}$	$\varepsilon_\parallel$	$r_{m\perp}$	$\varepsilon_\perp$	$A \cdot 10^5$
He	C-F	3.57	1.35	3.24	1.83	3.57	1.35	3.24	1.83	0
Ne	C-F	3.63	2.77	3.32	3.54	3.63	2.77	3.32	3.54	0
He	C-Cl	4.24	1.42	3.84	1.90	4.04	1.88	3.84	1.90	1.0
Ne	C-Cl	4.23	3.17	3.86	4.07	4.04	4.15	3.86	4.07	3.0
Ar	C-Cl	4.35	8.77	4.04	10.16	4.18	10.98	4.04	10.16	6.5

The parameters of each Ng-bond interaction contributing to V_{vdW}[58] were estimated by combining in the correlation formulas[65,66] the atomic polarizability of Ng (α_{He}= 0.2 Å^3, α_{Ne}= 0.4 Å^3, α_{Ar}= 1.64 Å^3)[77] with the polarizability tensor components of the C-Cl ($\alpha_\parallel$= 3.67 Å^3, $\alpha_\perp$= 2.08 Å^3) and C-F bond ($\alpha_\parallel$= 1.02 Å^3, $\alpha_\perp$=0.57 Å^3 for C-F), which relate to the dimension and shape of the electronic charge distribution around each bond[78], and are consistent with the molecular polarizabilities[77]. The obtained values were inserted in the ILJ formulation with the additional constraint that, at the long range, they furnished a global average attraction in agreement with that obtained using the dispersion coefficients reported by Kumar[79]. The obtained formulation of V was tested against the measured scattering data. As noted above, in the thermal collision energy range, the average component of $Q(v)$ and the oscillatory pattern provide complementary information on the intermolecular

interaction, being dependent on the scattering events at large and intermediate orbital angular momentum, respectively, which are directly affected by the strength of the long range attraction and by the features of the well depth[62–64].

For the analysis of atom-heavy molecule collisions, as those sampled in the present study, exact calculations of cross sections by close coupling methods become cumbersome, and would require a huge computational effort. However, it was demonstrated previously[80,81] that, in the thermal energy domain, the measured integral cross sections of atoms colliding with rotationally "hot" molecules, which exhibit a probability of inelastic events lower than that of rotationally "cold" ones, can be analyzed by an approximate semiclassical theoretical treatment[80,81]. The latter just applies to collisions at intermediate and large impact parameter (the classic equivalent of the orbital angular momentum), as those occurring in the present experiments, without losing any relevant information on the intermolecular interaction. Sustaining arguments are: *i*) the experimental observation, in atom-molecule collisions, of the absence of any appreciable quenching, due to the interaction anisotropy, of the glory amplitude when the mean molecular rotation time is comparable or shorter than the collision time[51,80–83]; *ii*) the suggestion from scattering experiments[51,80–84] and theory[80,81] that the interaction anisotropy becomes more effective, generating a glory quenching only when the collision velocity overcomes the value for which the collision time becomes significantly shorter than the molecular rotation time. Under such conditions, the projectile atom interacts with the molecule suddenly, i.e. the interacting complex tends to maintain "memory" of some specific configurations during each collision. In the present study, the collision dynamics was therefore confined within two distinct regimes, namely: *i*) a *spherical model*, where the molecule behaves as a pseudo-atom and the scattering is mostly elastic, and driven by a central (radial) field, and *ii*) an *anisotropic molecular model*, where the cross section is defined as a combination of independent contributions from limiting configurations of the collision complex (see e.g. refs.[57,74]). For the presently-investigated systems, we selected, in particular, three limit configurations, sampling three distinct regions of the PES, and representative of the interaction anisotropy. They describe, in particular, the intermolecular interaction when Ng approaches to the vertex (V_v), to the face (V_f) and to the edge (V_e) of the tetrahedral molecule. Accordingly, the two regimes selectively emerge as a function of the ratio between the mean rotation time, τ_M, required to probe an effective potential close to the isotropic component of the PES and the collision time τ_{coll}.

τ_M has been estimated as the time required to orient the approaching molecule in different limiting configurations of the collision complex ($\tau_M \simeq 10^{-12}$ and $\simeq 6\ 10^{-13}$ s for CCl_4 and CF_4, respectively, at T=300 K). τ_{coll} evaluated according to refs.[57,81], has been found to be varying with the beam velocity v between $\simeq 2\ 10^{-12}$ and $\simeq 5\ 10^{-13}$ s at v=0.5 and v=2.2 km/s, respectively. The time comparison suggests that CCl_4 can be considered as rotating sufficiently fast during the collisions only at low v ($v \leq 0.80$ km/s), while for CF_4 the same limit occurs for $v \leq 1.1$ km/s. Therefore, in the low velocity limit, the collisions have been considered exclusively elastic and mainly driven by an "effective" radial potential $V(R)$ (R is the intermolecular distance defined as the separation between the CM of two partners) related to the isotropic component of the PES, and obtained at each R by the average over the angular coordinates of the interaction. At higher velocity, i.e. when $\tau_{coll} << \tau_M$, the anisotropic molecular regime sets in. In this case, at each v, the individual cross sections, calculated from V_v, V_f and V_e, have been combined as illustrated in[58].

For Ng-CF_4, this dynamical treatment effectively reproduced the measured cross section (see Figures 1 and 3) simply exploiting the atom-bond representation of $V = V_{vdW}$, formulated with the zero order parameters, and without introducing further corrections. In particular, cross sections calculated from the selected cuts of the PES and from the spherical component are reported in Figure 3, together with those obtained combining them, according to the different dynamical regimes introduced above, in order to be compared with the experimental data. In such figure the cross sections are reported as $Q(v)v^{\frac{2}{5}}$ to make a more fine comparison, showing that the complete calculations reproduce both the amplitude and frequency of the observed glory pattern. This result represents an important reliability test of the used methodology, and indicates the pure vdW character of the interaction occurring in Ng-CF_4. Figure 4 plots the total potential energy V of He/Ne-CF4 as a function of the intermolecular distance (centers of mass separator) R, evaluated from the used parameterization for selected cuts of the PES and for the spherical component. Used to reproduce the experimental data measured for Ng-CCl_4, the same methodology proved to be inadequate. The glory structures calculated for such systems with the predicted parameters, in fact, invariably shifted at lower velocity with respect to the experimental ones (see e.g. the upper panel of Figure 5). Thus, in these systems, the main intermolecular interaction cannot be described as a vdW interaction, simply defined in terms of bond polarizability components. Any attempt to fit the experimental data by simply adjusting the V_{vdW}

parameters, even well outside reasonable limits suggested by the correlation formulas[65,66], was unsuccessful. The observed glory pattern have been reproduced only by adjusting the potential formulation so to include two additional contributions. Interestingly, both these terms have a clear chemical meaning, and reflect the peculiar electronic structure of CCl_4. The first one takes into account a more specific anisotropic character of the electron density in molecules containing heavier halogen atoms. It was suggested previously (see e.g ref.[11] and references therein) that along a carbon-halogen bond the halogen atom behaves as a "flattened sphere", originating a "polar flattening" (PF) zone, often also associated with a positive electrostatic potential, the so called "σ-hole". This zone originates an anisotropic distribution of charge density, not included in the present formulation of the vdW potential. To account for this contribution, we decreased the position of the repulsive wall of each Ng-bond pair in the parallel configuration by about 4%. In particular, the shift amounts to 0.16, 0.15, 0.14 Åfor He-, Ne-, Ar-CCl_4, respectively (for major details and[58]). The obtained effect was an increase of the potential well of the vertex geometries of Ng-CCl_4, that are those mainly probed by the present experiments (zero-order and final parameters of V_{vdW} are reported in Table I). As a consequence, the anisotropic size repulsion decreases, accompanied by an increased weight of the dispersion attraction. The PF correction to the Ng-CCl_4 atom-bond pairs was consistently included by decreasing the effective parallel polarizability component of the C-Cl bond[65,66]. It was, in particular, applied so to obtain a size change consistent with that extracted from the scattering experiments involving state-selected Cl atom beams and He or Ne[58,85]. These previous experiments demonstrated that the Cl-He and Cl-Ne interactions are essentially driven by V_{vdW}, and permitted to assay the difference (anisotropy) in strength and range that originates from the different alignment (parallel or perpendicular) of the half-filled orbital of Cl with respect to the interaction axis[85]. Further details are given in Figure S2 . We mention that our findings (i.e. the repulsive wall shifted of about 0.16-0.14 Å are fully consistent with the recent theoretical estimates of Ref.[28]. In any case, despite the correction for the anisotropy of the electron density somewhat improved the fitting of the experimental data (see upper panel of Figure 5, curve labelled as V_{vdw}+PF), it was insufficient to fully reproduce the measurements. Recently, we showed that CT effects play a significant role in the bond stabilization of various types of gas-phase binary complexes involving hydrogenated molecules[50,54,55]. We therefore decided to modify the Ng-CCl4 potential so to included a further conceivable stabilizing contribution arising

from CT (V_{CT}). This term, assumed to depend on the overlap integral between external orbitals of the interacting partners and therefore expected to be stereo-selective, has been formulated as a sum of four (number of atom-bond interaction terms) exponentials which decreases with the distance r_b (the distance from the Ng atom from the interaction center on each CX bond, b, of CX_4):

$$V_{CT} = -A \sum_b cos^4(\alpha_b)\, e^{-\gamma r_b} \ . \tag{2}$$

At each molecular orientation (obtained by fixing r_b and α_b, see above and[58] for details), the value of γ defines[86,87] the falloff of V_{CT} with the separation of Ng from the interaction center, and indirectly from the Cl atoms in CCl_4. It was taken as coincident with that obtained for Cl-heavier Ng atom complexes, where strength, range, and anisotropy of CT were so far explored in great detail[85–89]. Therefore, the best fit of the experimental cross sections required to adjust only the pre-exponential factor A (optimized values are reported in Table I). The cross sections calculated with the modified V are plotted as full lines in Figures 2 and 5. The lower panel of Figure 5 provides for Ne-CCl_4 both the cross sections calculated from different cuts of the proposed PES and their combination, according to the dynamical regimes adopted for the data analysis. Figure 6 reports different cuts of the PES for Ne-CCl_4 system, and emphasizes the role of the various components on the full interaction. Note that the global reduction of the repulsive wall position (due to PF plus CT) affects mostly the vertex configuration (about 0.4-0.5 Å) and that the PF correction accounts for ca. 1/3 of the full energy change (see also Figure S3). Finally, Figure 7 compares the full interaction occurring in He/Ne/Ar-CCl_4 systems in the three selected cuts of the PESs, and in their spherical terms. The comparison emphasizes the general increasing of the interaction, both at long range and in the well region, in going from He to Ar. In addition, in each case V_v and V_f exhibit the most and less long range attraction, whereas the potential well depth decreases in going from V_f to V_v. It is also interesting that the well features of the spherical component are mostly affected by the position and strength of the repulsive wall of V_v.

IV. THEORETICAL ANALYSIS

As discussed above, the sole anisotropic V_{vdw} component effectively reproduces only the measured cross sections of Ng-CF_4. To reproduce the glory patterns of the Ng-CCl_4 it was, instead, necessary to adjust the V_{vdw} parameters so to include the PF effect and to add explicitly an attractive contribution (of exponential form) arising at short range distances which is consistent with the presence of a certain amount of CT. In this section we present an extensive computational campaign, based on high-level ab-initio calculations, which allowed us to put these phenomenological modifications on a firmer ground.

A. Computational details

All calculations have been carried out at coupled cluster level of theory[90–92] with single, double (CCSD), and perturbatively included triple excitations (CCSD(T)) using augmented correlation consistent polarized valence basis set up to quintuple-ζ (aug-cc-pVxZ, referred as AVxZ with x=T, Q, 5)[93–95]. Complete basis set (CBS) extrapolated energy values have been also evaluated using a three points extrapolation procedure.[96] All calculations have been carried out using the parallel version of the program MOLPRO[97]. The relatively weak interaction with Ng leaves the geometries of CCl_4 and CF_4 essentially unaffected. Thus, during all the calculations, the C-Cl and C-F bonds were kept rigid at their equilibrium distances (1.776 Åand 1.315 Å, respectively)[98,99]. With frozen-geometry fragments and with additional constrain that Ng is allowed to move on the CCl_4 (CF_4) symmetry plane (isolated molecules present a T_d symmetry), the geometry of Ng-CCl_4 (CF_4) is defined in terms of the distance R between the Ng and the C atom (located at the molecular CM) and the angle ϕ between the Ng-C axis and the C_3 symmetry axis of CCl_4 (CF_4). To study the presence of a CT component in these systems, we analyzed the electron density changes due to the interaction between CCl_4(CF_4) and the Ngs by means of the charge-displacement function (CDF)[100], which we have successfully used to study intermolecular weak interactions[48,50,52–55,101,102] and chemical bonding in several diverse contexts[103–106].

B. Equilibrium structures and energetic stability of the Ng-CX_4

We focused our attention on those cuts of the PES showed to be relevant for the anisotropic behavior of the Ng-CX_4 (with X=F, Cl) interaction (referred as *vertex*, *edge* and *face* in the experimental section). With our choice of coordinates (see above), the *vertex* configuration is defined by $\phi = 0$ with the Ng approaching the CX_4 molecule along its symmetry axis and pointing directly to the halogen atom, the *edge* configuration is defined with $\phi = 54.7$ degrees with the Ng approaching the CX_4 molecule in the direction of the bisector of the angle between two C-X bonds and finally the *face* configuration, defined by $\phi = 180$, presents the Ng pointing directly to the C atom of CX_4 in the direction of its symmetry axis.

The optimized intermolecular distance (R) of these three configurations and the corresponding interaction energies (E) are reported for Ng-CCl_4 and Ng-CF_4 in Table II and III, respectively. The predicted R values are essentially independent on the basis set and agree very well with the experimental values (also reported in the tables and referred as "Exp.") extracted from the model of the PES adopted in the cross section data analysis. The largest deviation in R is of 0.3 Å for the *face* configuration of the He/Ne-CCl_4 systems. In the *vertex* and *edge* the deviations are even smaller, in all cases below 0.1 Å.

The calculations well reproduce the relative stabilities of the vertex, edge, and face configurations, and the strictly related trends between R and E. Thus, for any Ng, the vertex configuration (Φ= 0) results in a largest R, likely arising from a highest Pauli repulsion, and this reflects in a lowest E. In any case, according to the experimental findings, E progressively increases in the expected order He < Ne < Ar. The structures and stabilities of the He/Ne-CF_4 follow trends strictly similar to those obtained for the He/Ne/Ar-CCl_4, and they are again well reproduced by the calculations.

Obtaining highly accurate interaction energies for these weakly bound systems is challenging (in spite of the very large basis sets employed). The computed interaction energies tend to decrease with increasing basis set size up to the CBS extrapolated limit values. These reference data generally agree with the experimental data (Exp.) (differences below 1 meV) in the case of the CF_4 complexes whereas, in the case of CCl_4, tend to slightly overestimate the experimental results. In all cases the overestimation is below 20% of the total interaction energy and in absolute value tends to increase along the Ng series: the largest

deviations are of 1.5 meV, 2.7 meV and 7.7 meV (less than 0.2 kcal/mol) for He-CCl_4 (in vertex configuration), Ne-CCl_4 (face) and Ar-CCl_4 (face), respectively.

The level of accuracy required by the experiments presented here (of the order of the meV) needs, besides the use of very large basis sets, the highest accuracy in treatment of the electron correlation. The effect of triple excitations (included here at the perturbation level) in the Coupled Cluster expansion (CCSD(T)) gives a significant contribution (in some cases even more than 30%) to the total interaction energies. As example, in Table II (case of vertex configuration of Ar-CCl_4) we report a comparison between the interaction energies evaluated at CCSD(T) and CCSD level. The effect of including perturbative triple excitations is to reduce the interaction energy between Ar and CCl_4 of about 8 meV. It is remarkable that the experimental estimate falls at halfway of the CCSD(T) and CCSD results. One may expect that an explicit inclusion of the triple (or higher) excitations in the Coupled Cluster expansion (CCSDT, CCSDQ methods[107]) may contribute to achieve even more accurate results.

He-CCl_4						
basis	vertex		edge		face	
	R	E	R	E	R	E
AVTZ	5.0	6.8	4.4	5.7	3.8	8.9
AVQZ	5.0	5.6	4.4	5.4	3.8	7.6
AV5Z	5.0	5.4	4.4	5.4	3.8	7.3
CBS	5.0	5.1	4.4	5.1	3.8	7.2
Exp.	5.1	3.6	4.4	4.8	4.1	6.2
Ne-CCl_4						
basis	vertex		edge		face	
	R	E	R	E	R	E
AVTZ	5.1	14.0	4.3	14.1	3.8	21.0
AVQZ	5.1	12.5	4.3	13.4	3.8	19.0
AV5Z	5.1	11.1	4.3	12.4	3.8	17.4
CBS	5.0	9.7	4.4	11.4	3.8	16.0
Exp.	5.0	9.3	4.4	10.3	4.1	13.3
Ar-CCl_4						
basis	vertex		edge		face	
	R	E	R	E	R	E
AVTZ	5.3	28.8 (22.0)	4.6	31.8	4.1	44.0
AVQZ	5.3	27.3 (20.0)	4.6	30.4	4.1	41.7
AV5Z	5.3	27.0 (19.5)	4.6	30.8	4.1	42.4
CBS	5.3	24.6 (16.9)	4.6	29.3	4.1	41.2
Exp.	5.3	19.3	4.6	26.3	4.3	33.5

TABLE II. Computed geometrical parameter R (Å) and interaction energy E (meV) of He-, Ne- and Ar-CCl_4 at CCSD(T) level using different basis sets for three relative orientations (vertex, edge, face), see text for details (1 meV=0.02306 kcal/mol). The values of E extrapolated at complete basis set (CBS) limit are also reported as those obtained from the analysis of the experimental data (Exp.). In parenthesis are reported results obtained at CCSD level.

He-CF_4						
basis	vertex		edge		face	
	R	E	R	E	R	E
AVTZ	4.2	5.4	3.7	6.4	3.2	10.5
AVQZ	4.2	4.5	3.7	5.6	3.2	7.9
AV5Z	4.2	3.9	3.7	5.0	3.2	6.7
CBS	4.2	3.3	3.7	4.5	3.2	5.8
Exp.	4.2	2.5	3.6	5.1	3.4	6.3

Ne-CF_4						
basis	vertex		edge		face	
	R	E	R	E	R	E
AVTZ	4.3	11.2	3.7	21.0	3.3	21.0
AVQZ	4.3	9.7	3.7	17.7	3.3	17.7
AV5Z	4.3	7.5	3.7	14.4	3.4	14.6
CBS	4.3	5.2	3.7	11.4	3.4	11.7
Exp.	4.3	5.2	3.7	10.0	3.5	12.2

TABLE III. Computed geometrical parameter R (Å) and interaction energy E (meV) of He- and Ne-CF_4 at CCSD(T) level using different basis sets for three relative orientations (vertex, edge, face), see text for details. The values of E extrapolated at complete basis set (CBS) limit are also reported as those obtained from the analysis of the experimental data (Exp.).

C. Estimate of polar flattening of the halogen in the CX_4 molecules

In the analysis of our scattering experiments, we suggested that a significant stabilization of the vertex configuration for the Ng-CCl_4 systems arises from the shift, at shorter distance, of the position of the repulsive wall of the pure V_{vdW} model potential.[26–28] An empirical correction was introduced suggested by previous scattering experiments involving state-selected Cl atom beams and lighter Ngs (see section III) for details). The net effect was mainly the increasing of the potential well (almost exclusively) of the vertex configurations, and the decreasing of its equilibrium distance (in the range of 0.17-0.2 Å) and the shift of the repulsive wall of about 0.16-0.14 Å (see above and, as an example, Figure S3). This was mainly attributed to the effective shape of the Cl atom in CCl_4 molecule that is indeed expected to be flattened[8,23–28] in the outer region of halogen along the σ-bond in the direction of the approaching Ng.

In the following, we explore exactly this point by comparing the relevant features of the electronic density at the halogen site in the CCl_4 and CF_4 molecules with those of spherical symmetric densities of respective isolated halogen atoms. Our simple analysis is aimed to gain some quantitative information on the halogen effective shape in these simple covalent molecules.

In Figure 8 we compare the electron density profile of CX_4 molecule (solid line) along the C-X chemical bond (with X=F, Cl) with that of a spherical isolated halogen atom (dotted line), placed at the same position that X assumes in the molecule. The figure highlights the low density regions, in the outermost part of halogens, which are of interest for the polar flattening. For CCl_4, the flattening of halogen emerges clearly: the density profile of the CCl_4 molecule is indeed systematically lower than that of the isolated spherical Cl atom. Intuitively, this situation favors a closer approach of the noble gas along the C-Cl direction and a stronger close-range attractive interaction. We may expect that the shift in the position of the repulsion wall, suggested for the vertex configuration of the Ngs-CCl4 systems, has to be strictly related to the shift at lower distance of density profile of CCl_4. A measure of the shift may be provided by the Δz(Å) value, defined as the distance between two points of density profiles (one for CX_4 and the other for the isolated X halogen atom) taking the same density value. $\Delta z(\rho)$ assumes a narrow range of values considering suitable values along the density profile (lower panel of Figure 8). Δz values for CCl_4 and CF_4, at an

isodensity of 0.001 (e Bohr^{-3}), representing the molecular surface (this value of isosurface is typically used to map the Coulomb potential for studying the σ-hole[8,108]), are respectively of 0.18 Å and 0.04 Å. The values obtained for the CCl_4 system support, in particular, that the size repulsion component of V_{vdw}, probed by Ng approaching along the C-Cl bond, must be shifted at a shorter distance of about 0.15-0.2 Å. It is interesting to mention that a similar correction has been recently introduced in an advanced force field model specifically devised for biomolecular halogen-bonds.[28] This justifies the first empirical adjustment in the formulation of the intermolecular potential (see section III). In addition, the polar flattening effect is found to be significantly reduced (small values of Δz) in the CF_4 case. This is also consistent with the fact that our scattering experiments for CF_4 are well reproduced by the adopted potential model without an explicit adjustment of the size repulsion component.

D. Charge Transfer (CT) effects

To investigate the occurrence of CT in the Ng-CCl_4 and Ng-CF_4, including its radial dependence and stereo-specifity, we exploited the charge displacement function (CDF), recently employed with success to study the chemical bond in several contexts[103–106], including weak intermolecular hydrogen bonds[50,54,55]. CDF offers a broad perspective for an assessment of the CT occurrence, free of any charge decomposition scheme.

Briefly, the CDF is defined as:

$$\Delta q(z) = \int_{-\infty}^{\infty} dx \int_{-\infty}^{\infty} dy \int_{-\infty}^{z} \Delta\varrho(x, y, z')\, dz' \tag{3}$$

with $\Delta\rho$ being the difference between the electron density of the complex and that of the isolated constituting fragments Ng and CX_4, placed at the same position they occupy in the complex. At each point along a chosen axis z (identified here for convenience as the R direction, see before), Δq measures the net electron charge that, upon the formation of the complex, flows from right to left across the plane perpendicular to z. Thus, a negative Δq corresponds to a flux of charge from left to right. This provides a concise, but insightful snapshot, of the whole electron cloud rearrangement arising as the consequence of the intermolecular potential effect. The evaluation of $\Delta q(z)$ along an axis joining the two interacting species is immediately helpful for a qualitative assessment of occurrence and extent of CT, because the curve obviously suggests CT when it is appreciably different from zero and does

not change sign in the region between the fragments, whereas CT may be uncertain (in both magnitude and direction) if the curve crosses zero in the same region. When CT takes place, it is useful, for comparative purposes, to come up with some definite numerical estimate of it, which can simply be done by taking the value of the CDF curve at a specific point between the fragments. According to our previous work, we have conveniently chosen to separate the fragments and to extract the CT value at their so-called isodensity boundary, i.e., at the point along z where the electron densities of the non interacting fragments become equal. We presently employed the CCSD/aug-cc-pVTZ electron densities for all systems (it is well documented[50,102] that the CDF fast converge with the size of the basis set).

The results for He-, Ne- and Ar-CCl_4 are reported in Figures 9, 10 and 11, respectively. For each system, we considered the geometries corresponding to the vertex , edge and face configurations, and fixed the distance between fragments at the values mainly experimentally probed (see figures' captions for details).

Let's start with the analysis of the He-CCl_4 system at the vertex configuration (He points directly the Cl atom of the molecule). The 3D plot of the isodensity deformation $\Delta\rho$ clearly shows that CCl_4 polarizes the spherical cloud of He, which undergoes a depletion (red colour) in the region opposite to that pointing Cl, while a charge accumulation (blue colour) is evident toward the halogen atom. In this configuration a certain amount of charge rearrangement is present, even at the CCl_4 site. The result of our analysis for the other configurations (edge, face) reveals immediately a remarkably different pattern. In these cases, the isosurface of $\Delta\rho$ indicates that the density fluctuations are much less pronounced, even negligible at the CCl_4 site, while there is an inverted polarization at the He region. The Δq curves are crucial to quantify the changes in the in the three configurations taken into account. Specifically, they show immediately an important qualitative signature: at difference with the other two cases, in the vertex configuration the curve is distinctly positive everywhere over the whole complex, never approaching zero in the inter-fragment region. This is the most clear evidence of a net CT from He to CCl_4. More in detail, electrons start flowing to the left already on the right side of He, so that 2.4 me have moved across the site of the He nucleus. Further to the left, the CDF value decreases reaching a minimum. The position of the minimum is close to the isodensity boundary between the fragments, located at 3.5 Å from the carbon and 1.3 Å from He. At this point the Δq value, which we take as an estimate of CT from He to CCl_4, is of 0.7 me. After this, charge starts to re-accumulate,

CDF remains quite stable in the region of the C-Cl bond, decreasing to the zero value at the left side of CCl_4. The CT value is clearly not negligible and somewhat unexpected for this system taking into account the small size and the general inertness of He. This result clearly underlines the significant role of CT in the formation of weak intermolecular halogen bonds.

The pattern of CDF at the edge configuration of He-CCl_4 (central panel, Figure 9), is completely different from the above picture. Here, CDF is negative at the He site (indicating an opposite charge shift that is now from the left to the right of the He nucleus), it assumes very small positive values in the inter-fragment region and remains very close to zero in the whole region of CCl_4. CDF shows also a change of sign between the two fragments and then the contribution of CT, if present, becomes more hardly defined, and one may expect its role remains marginal. A similar behavior is also suggested by CDF obtained for the face configuration (lower panel, Figure 9). Also in this case one may expect the CT component does not play an effective role, at least at the intermolecular distances probed by the experiments. Again, one may expect that CT component does not play a role, with the attraction determined solely by the dispersion forces.

The CDF curves of the various configurations of both Ne-CCl_4 and Ar-CCl_4 complexes (see Figure10 and Figure11), are qualitatively very similar to those described above for He-CCl_4. At the vertex configurations, the CDF curves are invariably positive, and, at the isodensity boundary, the CT (in direction from Ng to CCl_4) amounts to 1.90 me and to 2.05 me for Ne-CCl_4 and Ar-CCl_4, respectively. It is noteworthy that these CT values are consistent (even larger) with those found in the Ng-water series.[102] In the edge and face configurations, the CT effects are again negligible. However, consistent with the higher electronic polarizability of Ne (0.40 $Å^3$) and Ar (1.64 $Å^3$), the polarization effects at the Ngs site appear more pronounced than those observed in He-CCl_4.

CT is expected to depend on the overlap between the electron clouds of the fragments and therefore it should fall off exponentially with distance. To explore this point, we examined the dependence of CT (the value of $\Delta q(z)$ at the isodensity boundary) on the Ng–CCl_4 inter-fragment distance (R). In particular, we evaluated the amount of CT within the range of the intermolecular distances R mainly probed by the present scattering experiment (4.2-5.2 Å). The analysis focused mostly on the vertex configurations (where CT is relevant) of the He/Ne/Ar-CCl_4 complexes.

The results are given in Figure 12, together with the plots obtained by exploiting of the equation

$$ln(CT) = ln(A_{CT}) - \gamma R \tag{4}$$

in which $ln(A_{CT})$ and γ have been extracted so to achieve the best reproduction of data. The linear dependence of $ln(CT)$ on R confirms the dependence of CT on the overlap integral between the fragments wavefunctions involved in the electron exchanging, a quantity which depends exponentially on R[86,87]. One also notes that the decay behaviors are strictly similar (the values of γ are 3.1, 2.8, 3.2 Å^{-1} for He-, Ne- and Ar-CCl_4, respectively). It is interesting that these values match fairly well with the exponential decay of the V_{CT} component, introduced in the potential formulation (see Eq. 2), where we fixed the parameter γ to 3.0 Å^{-1}.

This result is consistent with the simple expectation that, at least in the perturbative limit (i.e. when very small CT are involved), CT and the stabilization energy associated with it are proportional ($V_{CT} = k \cdot CT$).[30,101,109,110] A similar evidence was found in weak interacting systems as Ng-water[50]. The comparison of the CT obtained for He-, Ne- and Ar-CCl_4 with the respective experimental data analysis (Eq. 2 and Table I) allows an estimate of the constant k. The obtained k, are ca. -5.2, -5.8, -6.0 $\pm$1.5 eV/e for He, Ne and Ar-CCl_4. The associated global error ($\pm$1.5 eV/e) has been safely estimated considering the combined uncertainty in the V_{CT} (its pre-exponential factor A shows an error of 10-15%, see Eq. 2 and Table I) and in the separation between the PF and CT stabilization contributions. As shown above, even if the adopted model potential is strongly supported by first principle calculations just presented, a sharp separation between PF and CT can introduce an additional uncertainty in the k value. It is relevant to note that recently, Shaik et al.[30] proposed, exploiting extensive theoretical analysis on a variety of halogenated systems, a constant value consistent with the present estimate.

This analysis confirms that the CT effects are highly stereospecific, and affect the anisotropy of the PES. They must also be regarded as an additive component contributing mostly to stabilize the linear configurations ($\Phi = 0$) of the Ng-CCl_4 complexes.

Finally, the CDF curves for the vertex configuration of the He/Ne-CF_4, obtained at the Ng-C distance of 3.9 Å (mainly probed by the experiments), are shown in Figure 13. The polarization of Ng induced by CF_4 is opposite to that exerted by CCl_4, and the plots of CDF show changes of sign, that are suggesting of a strongly reduced role of CT (the CDF

curves of the Ng-CCl_4 are, instead, invariably positive for any z). As a matter of fact, the estimated values are small, and feature strongly attenuated not measurable effects.

V. CONCLUSIONS

Based on MB scattering experiments, we have resolved the quantum interference effects (the glory patterns) observed in the dependence of the integral cross section $Q(v)$ on the MB velocity v of the Ng-CCl_4 and Ng-CF_4 complexes. The experimental data, analyzed by a proper dynamical model, provided the absolute average intermolecular interaction energies, and unravelled features such as the potential anisotropy associated to some basic cuts of the full PESs. They have shown also the purely anisotropic vdW component of the interaction between He/Ne and CF_4. On the other hand, to reproduce the experimental findings of the He/Ne/Ar-CCl_4, two further terms had to be added to V_{vdW}. The first one reflects the "polar flattening" effect, and the second one accounts for a charge transfer between Ng and CCl_4, clearly observed also for the lightest and, in principle, most inert He. Both these contributions are particularly relevant for Ng approaching to the vertex of CCl_4. According to ab-initio calculations, the small anisotropy of the electron density of the apolar CCl_4 molecule is per se sufficient to enhance the CT, confirming its occurrence from Ng to the vertex of CCl_4. The same effect is, instead, not occurring with CF_4. Put in the context of the currently growing interest for the intermolecular halogen bonding as a motif connecting a variety of fields from materials science to structural biology[13,111,112], the experimental characterization of the absolute scale of the intermolecular interaction and of anisotropy effects at the halogen site may be of general relevance. In particular, the present characterization, in prototypical halogenated systems, of the shift of the V_{vdw} repulsive wall, and the ensuing increase of the dispersion attraction and CT effects, should allow a more rational design and proper formulation of new force fields[26].

REFERENCES

[1] A. Legon, Phys. Chem. Chem. Phys. **12**, 7736 (2010).

[2] R. S. Mulliken and W. B. Person, J. Am. Chem. Soc. **91**, 3409 (1969).

[3] O. Hassel, Science **170**, 497 (1970).

[4]G. R. Desiraju, P. S. Ho, L. Kloo, A. C. Legon, R. Marquardt, P. Metrangolo, P. Politzer, G. Resnati, and K. Rissanen, Pure & Applied Chemistry **85**, 1711 (2013).

[5]P. Metrangolo, G. Resnati, and G. Eds., Halogen Bondings: Fundamentals and Applications **Springer: Berlin** (2008).

[6]P. Metrangolo, H. Neukirch, T. Pilati, and G. Resnati, Acc. Chem. Res. **38**, 386 (2005).

[7]P. Metrangolo, Y. Carcenac, M. Lahtinen, T. Pilati, K. Rissanen, A. Vij, and G. Resnati, Science **323**, 1461 (2009).

[8]T. Clark, M. Hennemann, J. S. Murray, and P. Politzer, Journal of Molecular Modeling **13**, 291 (2007).

[9]P. Metrangolo and G. Resnati, Chem. Eur. J. **7**, 2511 (2001).

[10]J.-W. Zou, Y.-J. Jiang, M. Guo, G.-X. Hu, B. Zhang, H.-C. Liu, and Q.-S. Yu, Chem. Eur. J. **11**, 740 (2005).

[11]P. Politzer, P. Lane, M. C. Concha, Y. Ma, and J. S. Murray, Journal of molecular modeling **13**, 305 (2007).

[12]P. Metrangolo, F. Meyer, T. Pilati, G. Resnati, and G. Terraneo, Angew. Chem. Int. Ed. **47**, 6114 (2008).

[13]P. Metrangolo and G. Resnati, Science (New York, NY) **321**, 918 (2008).

[14]E. Arunan, Current Science **105**, 892 (2013).

[15]D. Mani and E. Arunan, Phys. Chem. Chem. Phys. **15**, 14377 (2013).

[16]K. E. Riley and P. Hobza, Phys. Chem. Chem. Phys. **15**, 17742 (2013).

[17]M. Kolář, J. Hostaš, and P. Hobza, Phys. Chem. Chem. Phys. **16**, 9987 (2014).

[18]C. Wang, D. Danovich, Y. Mo, and S. Shaik, J. Chem. Theory Comput. **10**, 3726 (2014).

[19]P. Politzer, J. S. Murray, and P. Lane, Int. J. Quantum Chem. **107**, 3046 (2007).

[20]J. S. Murray, P. Lane, and P. Politzer, Journal of Molecular Modeling **15**, 723 (2009).

[21]P. Politzer, K. E. Riley, F. A. Bulat, and J. S. Murray, Computational and Theoretical Chemistry **998**, 2 (2012).

[22]P. Politzer, J. S. Murray, and T. Clark, Phys. Chem. Chem. Phys. **15**, 11178 (2013).

[23]S. C. Nyburg, Acta Crystallographica Section A **35**, 641 (1979).

[24]F. F. Awwadi, R. D. Willett, K. A. Peterson, and B. Twamley, Chem. Eur. J. **12**, 8952 (2006).

[25]S. Peebles, P. Fowler, and A. Legon, Chem. Phys. Lett. **240**, 130 (1995).

[26]M. Carter, A. K. Rappé, and P. S. Ho, J. Chem. Theory Comput. **8**, 2461 (2012).

[27]A. El Kerdawy, J. S. Murray, P. Politzer, P. Bleiziffer, A. Hesselmann, A. Grling, and T. Clark, J. Chem. Theory Comput. **9**, 2264 (2013).

[28]M. R. Scholfield, M. C. Ford, C. M. Vander Zanden, M. M. Billman, P. S. Ho, and A. K. Rapp, **0**, null (0), aSAP.

[29]L. P. Wolters, P. Schyman, M. J. Pavan, W. L. Jorgensen, F. M. Bickelhaupt, and S. Kozuch, Wiley Interdisciplinary Reviews: Computational Molecular Science **4**, 523 (2014).

[30]C. Wang, D. Danovich, Y. Mo, and S. Shaik, J. Chem. Theory Comput. **10**, 3726 (2014).

[31]A. J. Stone, J. Am. Chem. Soc. **135**, 7005 (2013).

[32]S. M. Huber, E. Jimenez-Izal, J. M. Ugalde, and I. Infante, Chem. Commun. **48**, 7708 (2012).

[33]S. M. Huber, J. D. Scanlon, E. Jimenez-Izal, J. M. Ugalde, and I. Infante, Phys. Chem. Chem. Phys. **15**, 10350 (2013).

[34]M. Musso, H. Torii, P. Ottaviani, A. Asenbaum, and M. G. Giorgini, J. Phys. Chem. A **106**, 10152 (2002).

[35]F. Aliotta, M. Musso, R. Ponterio, F. Saija, and G. Salvato, **108**, 12972 (2004).

[36]P. Metrangolo, C. Präsang, G. Resnati, R. Liantonio, A. C. Whitwood, and D. W. Bruce, Chem. Comm. , 3290 (2006).

[37]G. Ciancaleoni, R. Bertani, L. Rocchigiani, P. Sgarbossa, C. Zuccaccia, and A. Macchioni, Chem. Eur. J. **21**, 440 (2015).

[38]P. Murray-Rust and W. S. Motherwell, J. Am. Chem. Soc. **101**, 4374 (1979).

[39]P. Murray-Rust, W. C. Stallings, C. T. Monti, R. K. Preston, and J. P. Glusker, J. Am. Chem. Soc. **105**, 3206 (1983).

[40]N. Ramasubbu, R. Parthasarathy, and P. Murray-Rust, J. Am. Chem. Soc. **108**, 4308 (1986).

[41]S. E. Novick, K. C. Janda, and W. Klemperer, J. Chem. Phys. **65**, 5115 (1976).

[42]A. Rohrbacher, K. C. Janda, L. Beneventi, P. Casavecchia, and G. G. Volpi, J. Phys. Chem. A **101**, 6528 (1997).

[43]J. A. Goodnough, L. Goodrich, and T. C. Farrar, J. Phys. Chem. A **111**, 6146 (2007).

[44]T.-M. Chang and L. X. Dang, J. Phys. Chem. A **112**, 1694 (2008).

[45]K. Mierzwicki, Z. Mielke, M. Saldyka, S. Coussan, and P. Roubin, Phys. Chem. Chem. Phys. **10**, 1292 (2008).

[46]W. Caminati, A. Maris, A. Dell'Erba, and P. G. Favero, Angewandte Chemie **118**, 6863 (2006).

[47]G. Feng, L. Evangelisti, N. Gasparini, and W. Caminati, Chem. Eur. J. **18**, 1364 (2012).

[48]D. Cappelletti, P. Candori, F. Pirani, L. Belpassi, and F. Tarantelli, Crystal Growth & Design **11**, 4279 (2011).

[49]R. Bernstein and T. O'Brien, Discuss. Faraday Soc. **40**, 35 (1965).

[50]D. Cappelletti, E. Ronca, L. Belpassi, F. Tarantelli, and F. Pirani, Acc. Chem. Res. **45**, 1571 (2012).

[51]L. F. Roncaratti, L. Belpassi, D. Cappelletti, F. Pirani, and F. Tarantelli, J. Phys. Chem. A **113**, 15223 (2009).

[52]F. Pirani, L. F. Roncaratti, L. Belpassi, F. Tarantelli, and D. Cappelletti, J. Chem. Phys. **135**, 194301 (2011).

[53]G. Bistoni, L. Belpassi, F. Tarantelli, F. Pirani, and D. Cappelletti, J. Phys. Chem. A **115**, 14657 (2011).

[54]F. Pirani, D. Cappelletti, L. Belpassi, and F. Tarantelli, J. Phys. Chem. A **117**, 12601 (2013).

[55]A. Bartocci, D. Cappelletti, F. Pirani, F. Tarantelli, and L. Belpassi, J. Phys. Chem. A **118**, 6440 (2014).

[56]D. Cappelletti, A. Bartocci, F. Grandinetti, S. Falcinelli, L. Belpassi, F. Tarantelli, and F. Pirani, Chem. Eur. J. **21**, 6234 (2015).

[57]D. Cappelletti, M. Bartolomei, F. Pirani, and V. Aquilanti, J. Phys. Chem. A **106**, 10764 (2002).

[58] Supplemental material at [URL will be inserted by AIP], .

[59]V. Aquilanti, G. Liuti, F. Pirani, F. Vecchiocattivi, and G. G. Volpi, J. Chem. Phys. **65**, 4751 (1976).

[60]T. Nenner, H. Tien, and J. B. Fenn, J. Chem. Phys. **63**, 5439 (1975).

[61]F. Pirani and F. Vecchiocattivi, J. Chem. Phys. **66**, 372 (1977).

[62]F. Pirani and F. Vecchiocattivi, Mol. Phys. **45**, 1003 (1982).

[63]F. Pirani, S. Brizi, L. F. Roncaratti, P. Casavecchia, D. Cappelletti, and F. Vecchiocattivi, Phys. Chem. Chem. Phys. **10**, 5489 (2008).

[64]M. Child, Molecular collision theory **Academic Press London and New York** (1974).

[65]R. Cambi, D. Cappelletti, G. Liuti, and F. Pirani, J. Chem. Phys. **95**, 1852 (1991).

[66]F. Pirani, D. Cappelletti, and G. Liuti, Chem. Phys. Lett. **350**, 286 (2001).

[67]F. Pirani, M. Alberti, A. Castro, M. M. Teixidor, and D. Cappelletti, Chem. Phys. Lett. **394**, 37 (2004).

[68]M. Alberti, A. Aguilar, J. M. Lucas, F. Pirani, D. Cappelletti, C. Coletti, and N. Re, J. Phys. Chem. A **110**, 9002 (2006).

[69]M. Alberti, A. Aguilar, J. M. Lucas, F. Pirani, C. Coletti, and N. Re, J. Phys. Chem. A **113**, 14606 (2009).

[70]M. Alberti, A. Amat, F. De Angelis, and F. Pirani, **117**, 7065 (2013).

[71]M. Bartolomei, E. Carmona-Novillo, M. I. Hernández, J. Campos-Martínez, and F. Pirani, **117**, 10512 (2013).

[72]M. Alberti, A. Castro, A. Lagana', F. Pirani, M. Porrini, and D. Cappelletti, Chem. Phys. Lett. **392**, 514 (2004).

[73]J. Marques, J. L. Llanio-Trujillo, M. Albertí, A. Aguilar, and F. Pirani, J. Phys. Chem. A **117**, 8043 (2013).

[74]M. Capitelli, D. Cappelletti, G. Colonna, C. Gorse, A. Laricchiuta, G. Liuti, S. Longo, and F. Pirani, Chem. Phys. **338**, 62 (2007).

[75]H. Werner and W. Meyer, Phys. Rev. A **13**, 13 (1976).

[76]E.-A. Reinsch and W. Meyer, Phys. Rev. A **14**, 915 (1976).

[77]T. N. Olney, N. Cann, G. Cooper, and C. Brion, Chem. Phys. **223**, 59 (1997).

[78]K. Denbigh, Transactions of the Faraday Society **36**, 936 (1940).

[79]A. Kumar, Journal of Molecular Structure Theochem **591**, 91 (2002).

[80]V. Aquilanti, L. Beneventi, G. Grossi, and F. Vecchiocattivi, J. Chem. Phys. **89**, 751 (1988).

[81]V. Aquilanti, D. Ascenzi, D. Cappelletti, M. de Castro, and F. Pirani, J. Chem. Phys. **109**, 3898 (1998).

[82]E. Luzzatti, F. Pirani, and F. Vecchiocattivi, Mol. Phys. **34**, 1279 (1977).

[83]F. Pirani, F. Vecchiocattivi, J. J. H. van den Biesen, and C. J. N. van den Meijdenberg, J. Chem. Phys. **75**, 1042 (1981).

[84]D. Cappelletti, P. Candori, S. Falcinelli, M. Alberti, and F. Pirani, Chem. Phys. Lett. **545**, 14 (2012).

[85]V. Aquilanti, D. Cappelletti, V. Lorent, E. Luzzatti, and F. Pirani, J. Phys. Chem. **97**, 2063 (1993).

[86]F. Pirani, A. Giulivi, D. Cappelletti, and V. Aquilanti, Molecular Physics **98**, 1749 (2000).

[87]V. Aquilanti, D. Cappelletti, and F. Pirani, Chemical Physics Letters **271**, 216 (1997).

[88]V. Aquilanti, D. Cappelletti, and F. Pirani, J. Chem. Soc., Faraday Trans. **89**, 1467 (1993).

[89]V. Aquilanti, D. Cappelletti, V. Lorent, E. Luzzatti, and F. Pirani, **192**, 153 (1992).

[90]K. Raghavachari, G. W. Trucks, J. A. Pople, and M. Head-Gordon, Chem. Phys. Lett. **157**, 479 (1989).

[91]C. Hampel, K. A. Peterson, and H.-J. Werner, Chem. Phys. Lett. **190**, 1 (1992).

[92]M. J. O. Deegan and P. J. Knowles, Chem. Phys. Lett. **227**, 321 (1994).

[93]T. H. Dunning, J. Chem. Phys. **90**, 1007 (1989).

[94]D. E. Woon and T. H. Dunning, J. Chem. Phys. **100**, 2975 (1994).

[95]D. E. Woon and T. H. Dunning, J. Chem. Phys. **98**, 1358 (1993).

[96]F. Jensen, Theo. Chem. Acc. **113**, 267 (2005).

[97]H. Werner, P. Knowles, R. Lindh, F. Manby, and M. Schütz, MOLPRO version 2012.1 a package of ab initio programs 2012 see http://www. molpro. net **1**, 1 (2012).

[98]H. Tachikawa, J. Phys. Chem. A **101**, 7454 (1997).

[99]S. Brodersen, Journal of Molecular Spectroscopy **145**, 331 (1991).

[100]L. Belpassi, I. Infante, F. Tarantelli, and L. Visscher, J. Am. Chem. Soc. **130**, 1048 (2008).

[101]L. Belpassi, M. L. Reca, F. Tarantelli, L. F. Roncaratti, F. Pirani, D. Cappelletti, A. Faure, and Y. Scribano, J. Am. Chem. Soc. **132**, 13046 (2010).

[102]L. Belpassi, F. Tarantelli, F. Pirani, P. Candori, and D. Cappelletti, Phys. Chem. Chem. Phys. **11**, 9970 (2009).

[103]N. Salvi, L. Belpassi, and F. Tarantelli, Chem. Eur. J. **16**, 7231 (2010).

[104]D. Zuccaccia, L. Belpassi, A. Macchioni, and F. Tarantelli, Eur. J. Inorg. Chem. **2013**, 4121 (2013).

[105]G. Bistoni, L. Belpassi, and F. Tarantelli, Angw. Chem. Int. Ed. **52**, 11599 (2013).

[106]G. Ciancaleoni, L. Biasiolo, G. Bistoni, A. Macchioni, F. Tarantelli, D. Zuccaccia, and L. Belpassi, Chem. Eur. J. **21**, 2467 (2015).

[107]M. Kállay and Surján, J. Chem. Phys. **115**, 2945 (2001).

[108]K. Riley, J. Murray, J. Fanfrlk, J. ez, R. Sol, M. Concha, F. Ramos, and P. Politzer, Journal of Molecular Modeling **19**, 4651 (2013).

[109]A. E. Reed, L. A. Curtiss, and F. Weinhold, Chem. Rev. **88**, 899 (1988).

[110]R. Z. Khaliullin, A. T. Bell, and M. Head-Gordon, J. Chem. Phys. **128**, 184112 (2008).

[111]M. Erdelyi, Nat. Chem. **6**, 762 (2014).

[112]A. R. Voth, P. Khuu, K. Oishi, and P. S. Ho, Nat. Chem. **1**, 74 (2009).

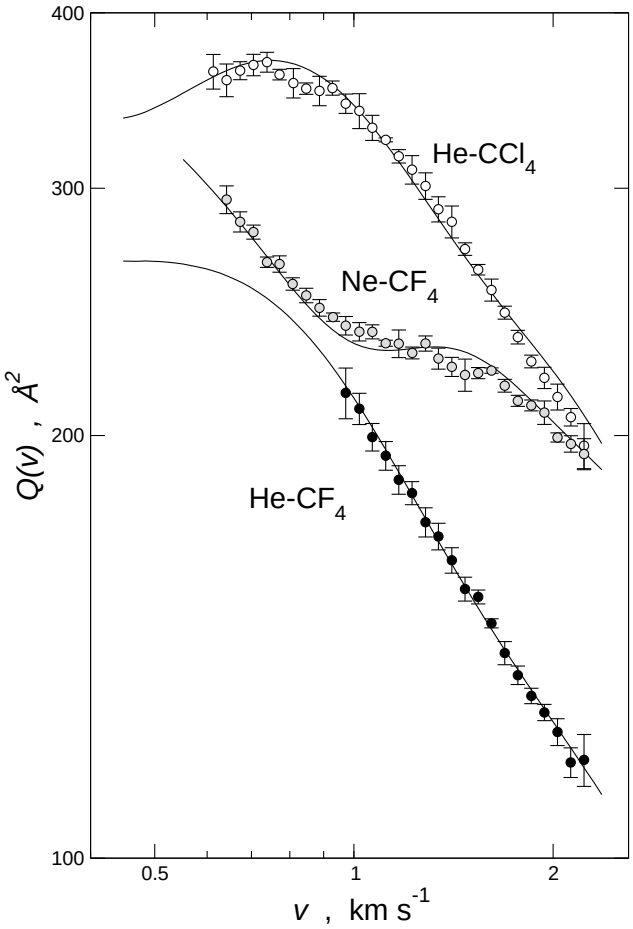

FIG. 1. Integral cross section $Q(v)$ for the He,Ne-CF_4 and He-CCl_4 systems measured as a function of the MB velocity v. As usual, vertical error bars represent $\pm$ two standard deviations from the average of typical term of measurements. The full lines represent the results of the best fit calculations (see text).

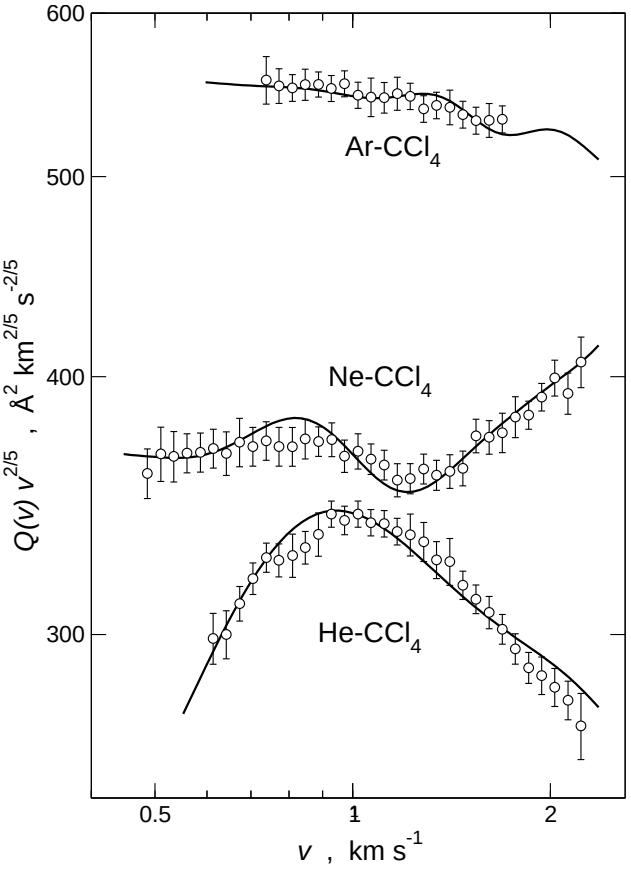

FIG. 2. Integral cross section, reported as $Q(v)v^{\frac{2}{5}}$, for the Ng-CCl_4 systems (with Ng=He,Ne,Ar) plotted as a function of the MB velocity v. As usual, vertical error bars represent ± two standard deviations from the average of typical term of measurements. The full lines represent the results of the best fit calculations (see text).

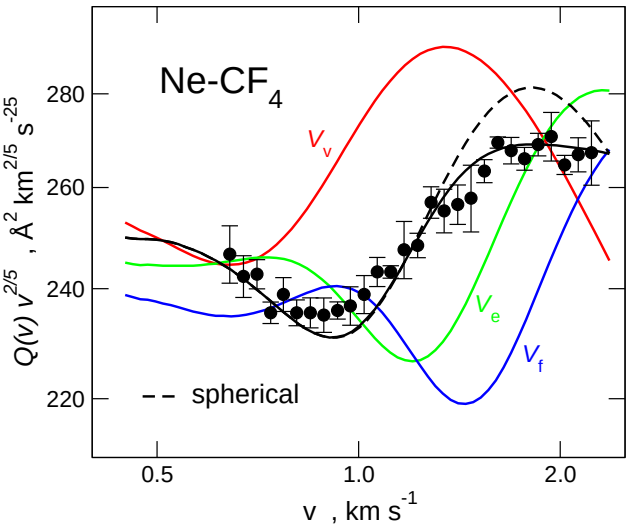

FIG. 3. Comparison for Ne-CF_4 system between the experimental cross section data, plotted as $Q(v)v^{\frac{2}{5}}$ (black circles) and reported as a function of the MB velocity v, and calculations (lines) performed with the proposed interaction and by considering the dynamical regimes discussed in the text. The separated contributions, arising from different cuts of the PES and from its isotropic component, are also shown.

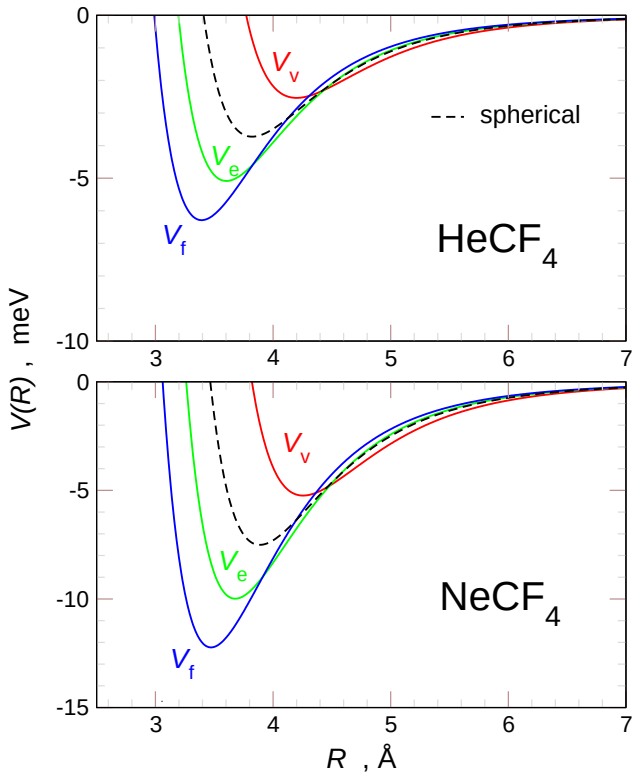

FIG. 4. The interaction energies V, plotted as a function of the intermolecular distance R, for three basic configurations (vertex, edge and face geometries) of the He-CF_4 and Ne-CF_4 complexes (upper and lower panel, respectively) and for the spherical term (the dashed lines curves) of the PES, as obtained by using only the V_{vdW} component (see text).

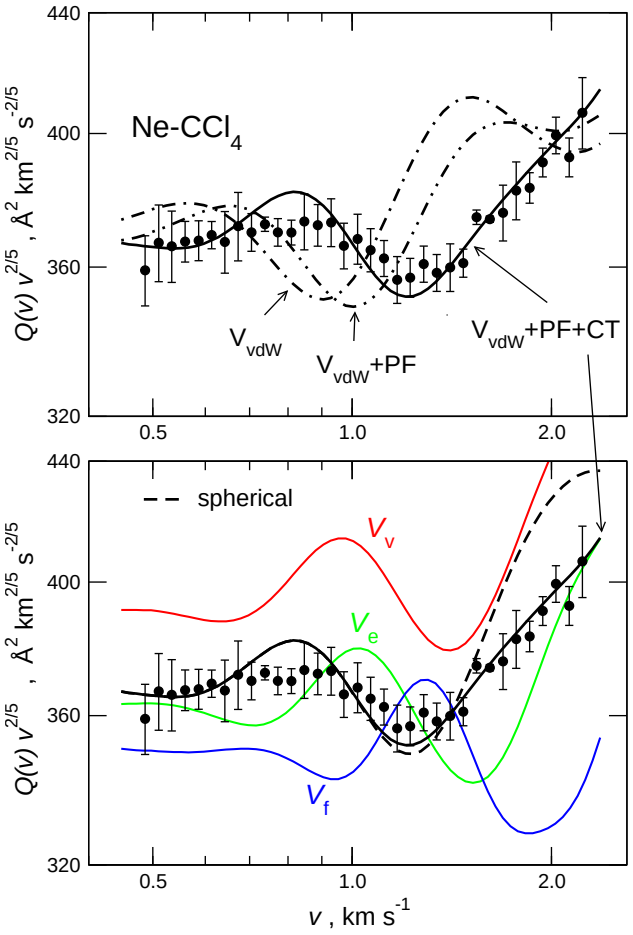

FIG. 5. Upper panel: comparison for Ne-CCl_4 system between the experimental cross section data, plotted as $Q(v)v^{\frac{2}{5}}$ (black circles) and reported as a function of the MB velocity v, and calculations carried out including in the potential formulation the various interaction contributions taken into account (see text). Lower panel: cross section contributions provided by different cuts of the PES and from its isotropic component are reported as separated and as combined according to the different dynamical regimes discussed in the text and detailed in SI.

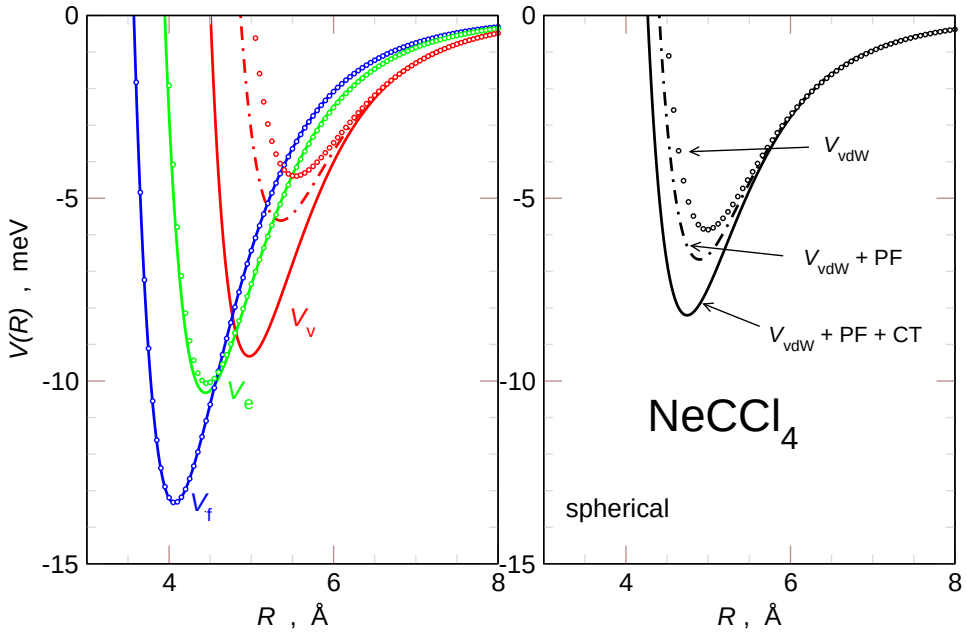

FIG. 6. In the left panel are shown the interaction energies V as a function of the distance R, evaluated for three basic configurations of the complex (vertex, edge and face geometries) and, in the rigth panel, for the spherical term of the PES, obtained using only the V_{vdW} component (dotted lines) (see Eqs. 4-7 in SI) and including also PF (dashed dotted lines) and CT effects (full lines).

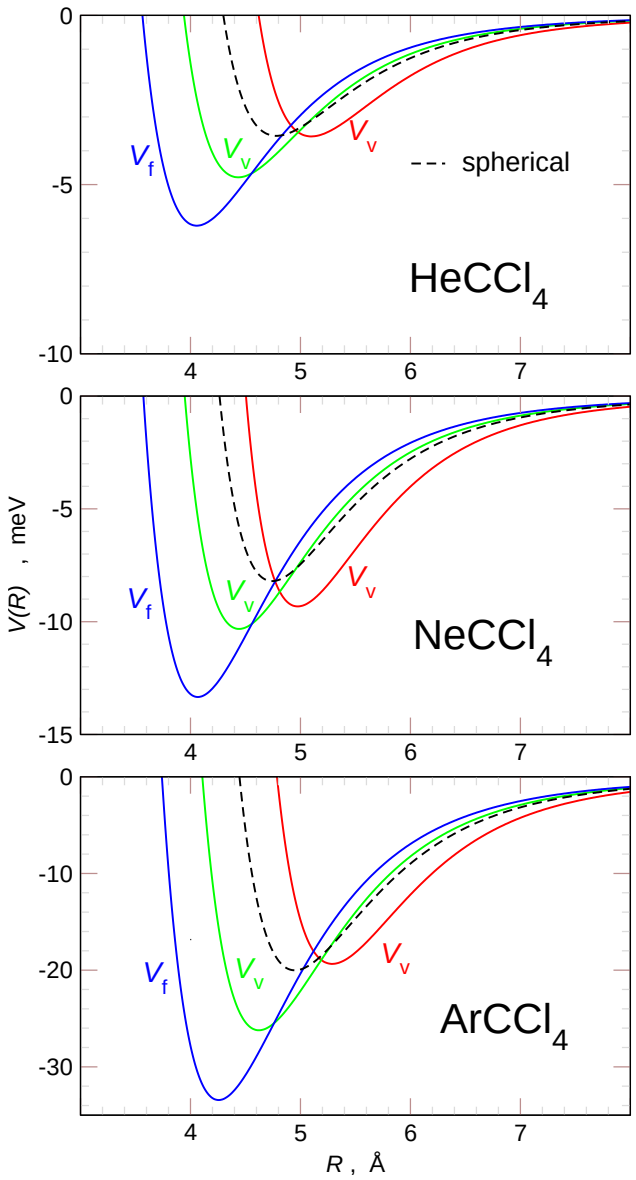

FIG. 7. The full interaction $V(R)$ plotted as a function of the intermolecular distance R for the selected cuts of the PES and with their spherical component for the Ng-CCl_4 systems. The dot-dashed line represent the interaction energy evaluated for the vertex (v), the dashed line for the edge (e), the full line for the face (f) and the open dots for the spherical component.

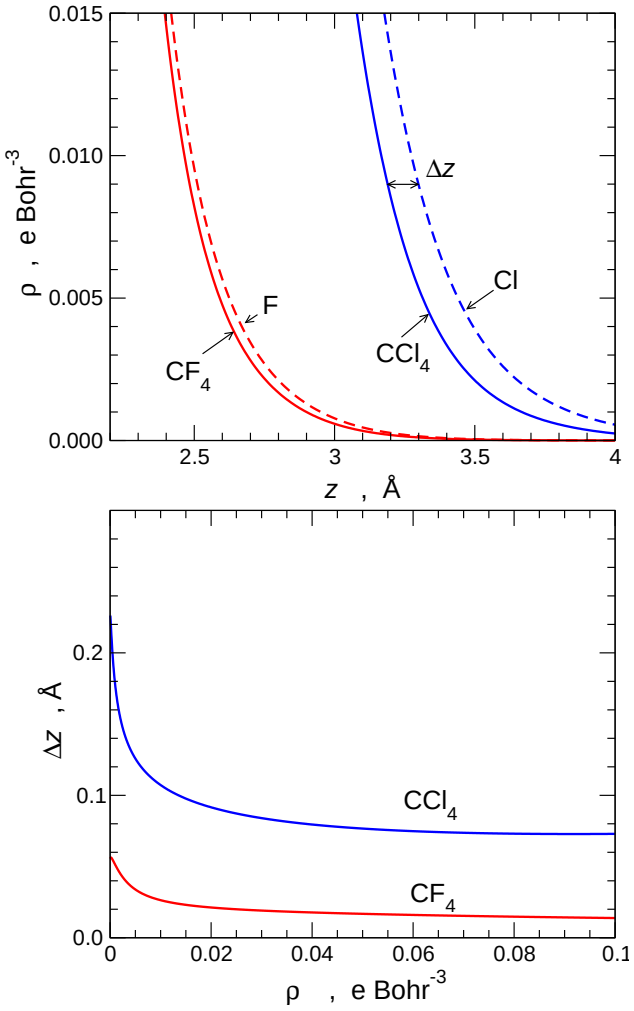

FIG. 8. In the upper panel, the electron density profile, ρ (e Bohr^{-3}), along the C-Cl (C-F) bond of CCl_4 (CF_4) molecule and of the spherical Cl (F) atom (dotted lines), placed at the same position which assumes in the molecule. In the lower panel, Δz (Å) behavior for the Cl/CCl_4 (solid line) and for F/CF_4 (dotted line) systems reported as a function of the density value (ρ), see text for details.

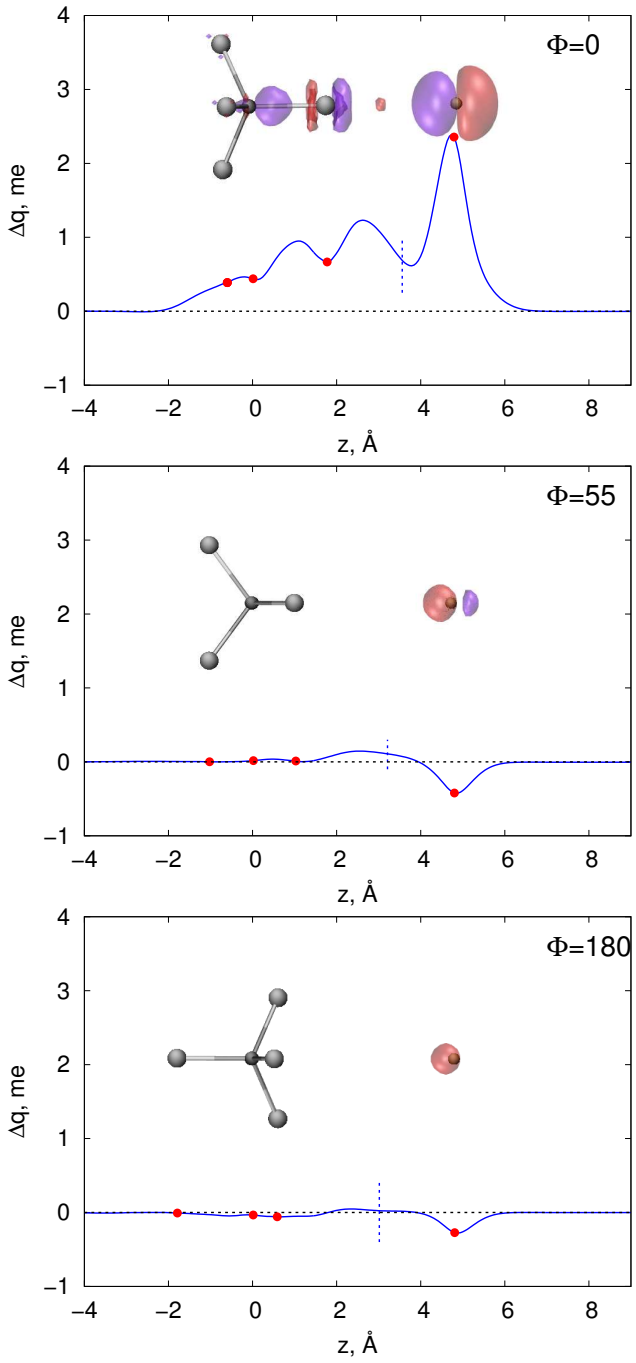

FIG. 9. CDF curves for three configurations of the CCl_4-He system (see text): Φ=0, Φ=55 and Φ=180. The 3D isodensity plots of the electron density change accompanying bond formation are also shown, with isodensity surfaces for $\Delta\rho\pm$ 5e-05 e/bohr^3. The dots on the Δq curves mark the projection of the nuclear positions. z origin is at the CCl_4's carbon atom C, while the He is placed at the experimental averaged distance (4.8 Å) from the C. The vertical dashed lines correspond to the isodensity boundaries between the fragments where CT has been evaluated.

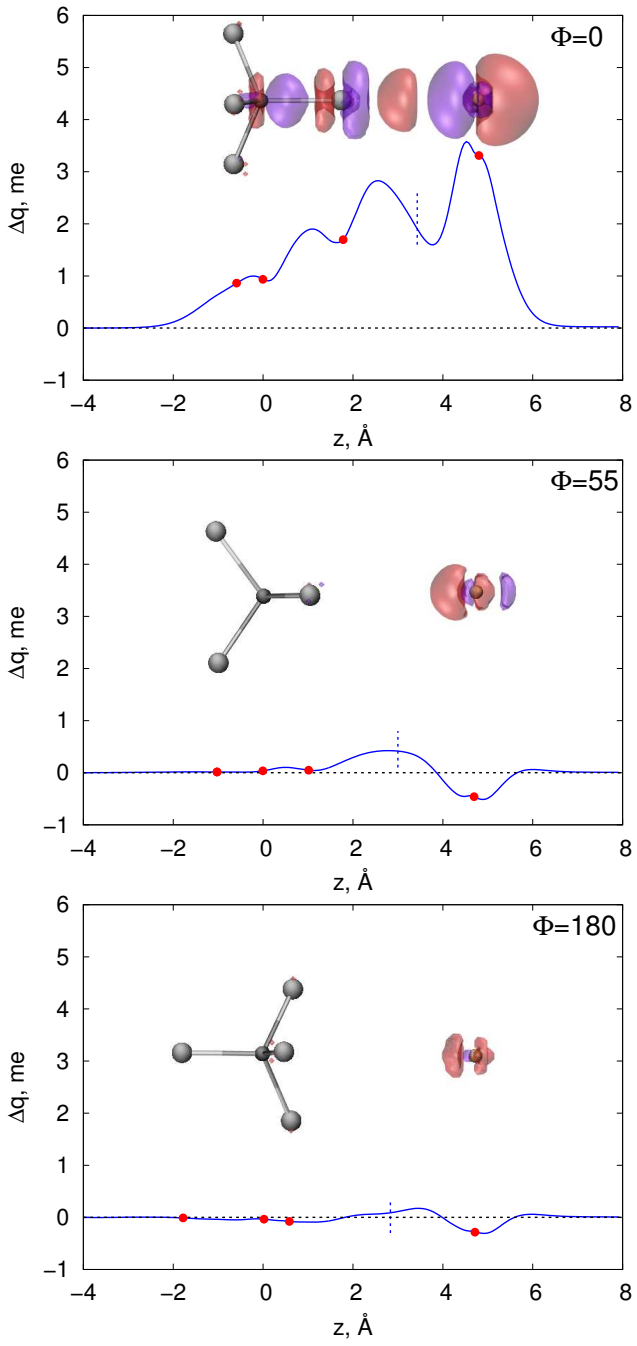

FIG. 10. CDF curves for three configurations of the CCl_4-Ne system (see text): Φ=0, Φ=55 and Φ=180. 3D isodensity plots of the electron density change accompanying bond formation are also shown, with isodensity surfaces for $\Delta\rho\pm$ 5e-05 e/bohr^3. The dots on the Δq curves mark the projection of the nuclear positions. z origin is at the CCl_4's carbon atom C, while the Ne is placed at the experimental averaged distance (4.8 Å) from the C. The vertical dashed lines correspond to the isodensity boundaries between the fragments where CT has been evaluated.

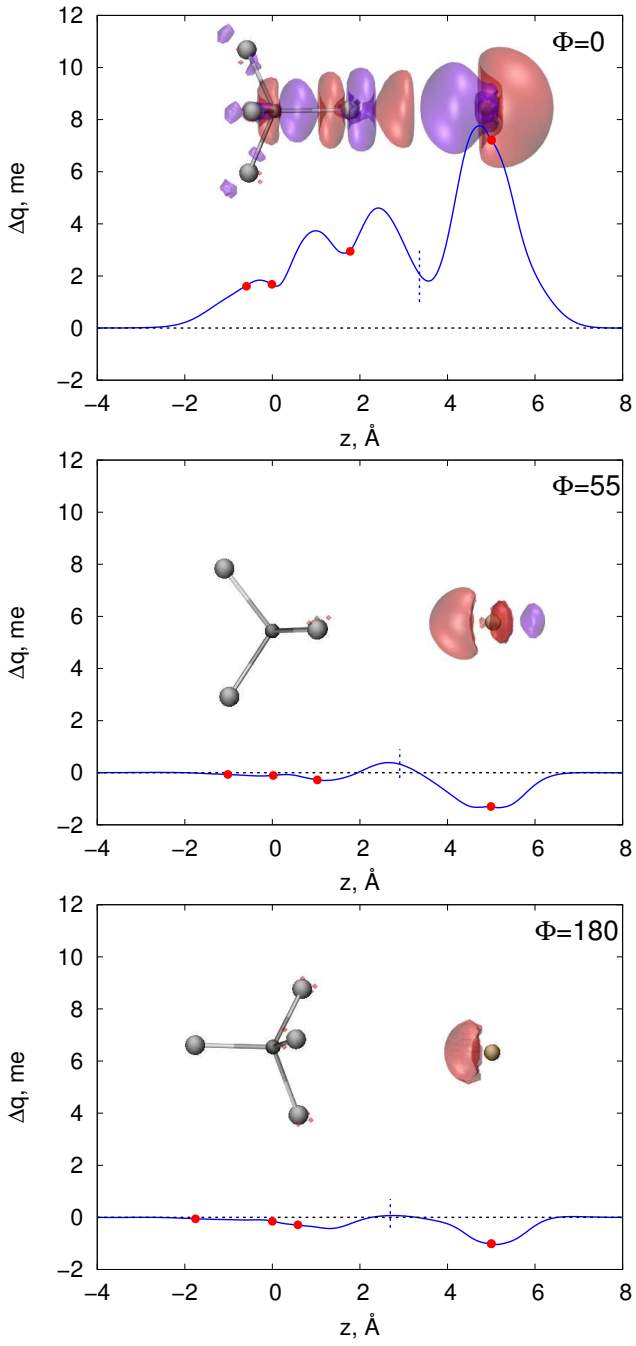

FIG. 11. CDF curves for three configurations of the CCl_4-Ar system (see text): Φ=0, Φ=55 and Φ=180. 3D isodensity plots of the electron density change accompanying bond formation are also shown, with isodensity surfaces for $\Delta\rho\pm$ 5e-05 e/bohr^3. The dots on the Δq curves mark the projection of the nuclear positions. z origin is at the CCl_4's carbon atom C, while the Ar is placed at the experimental distance (5.0 Å) from the C. The vertical dashed lines correspond to the isodensity boundaries between the fragments where CT has been evaluated.

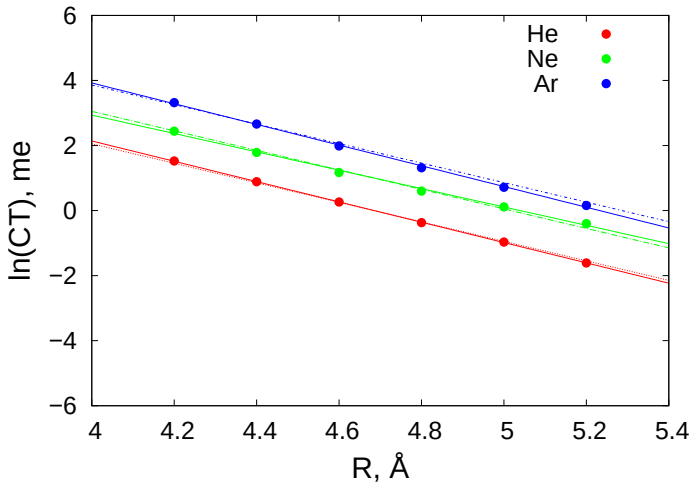

FIG. 12. ln(CT) (me) in function of the inter-fragments distance R for the vertex configuration ($\Phi = 0$) of the CCl_4-Ng systems (with Ng=He,Ne,Ar). The best fitting of the data (solid lines) done using the eq. 4 (with A_{CT} and γ as free parameters) and fixing γ=3.0 $Å^{-1}$ (dashed lines) are also shown in figure (see text for details) .

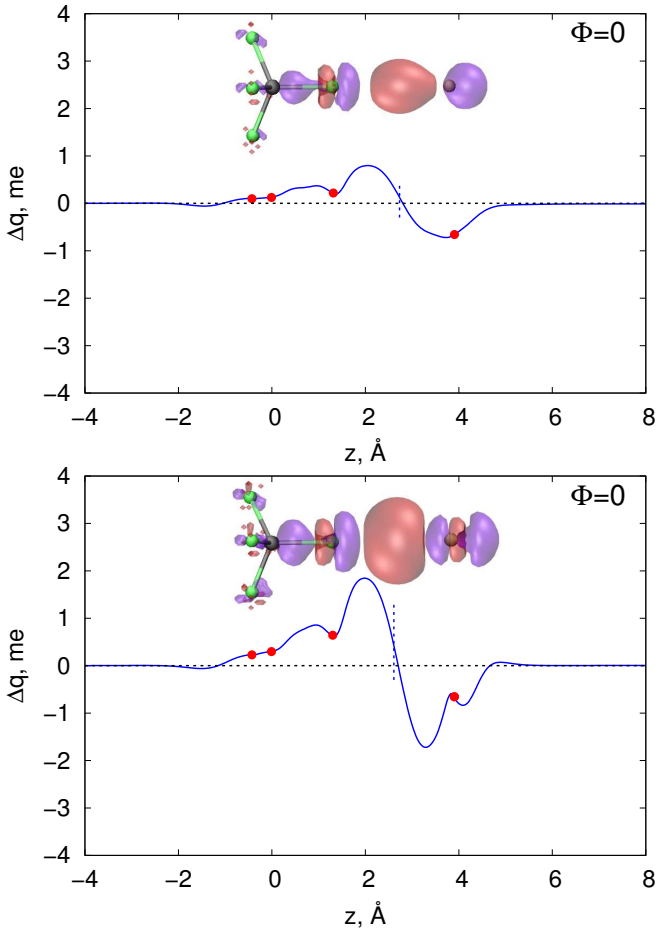

FIG. 13. CDF curves for the vertex configuration (Φ=0) of the CF_4-He (upper panel) and CF_4-Ne (lower panel) systems. 3D isodensity plots of the electron density change accompanying bond formation are also shown, with isodensity surfaces for $\Delta\rho\pm$ 5e-05 e/bohr^3. The dots on the Δq curves mark the projection of the nuclear positions. z origin is at the CF_4's carbon atom C, while the Ng is placed at the experimental distance (3.9 Å) from the C. The vertical dashed lines correspond to the isodensity boundaries between the fragments.